JOURNAL OF GEOPHYSICAL RESEARCH, VOL. 111, B12S35, doi:10.1029/2006JB004715, 2006

Characterization of hematite (α-Fe_2O_3), goethite (α-FeOOH), greigite (Fe_3S_4), and pyrrhotite (Fe_7S_8) using first-order reversal curve diagrams

Andrew P. Roberts,[1] Qingsong Liu,[1] Christopher J. Rowan,[1] Liao Chang,[1] Claire Carvallo,[1,2] José Torrent,[3] and Chorng-Shern Horng[4]

Received 25 August 2006; revised 30 October 2006; accepted 6 November 2006; published 16 December 2006.

[1] First-order reversal curve (FORC) diagrams have become a standard tool in rock magnetism, yet magnetite is the only magnetic mineral that is well characterized using FORC diagrams. We present FORC diagrams for predominantly single-domain (SD) synthetic aluminous hematite (α-$Fe_{2-x}Al_xO_3$) and goethite (α-(FeAl)OOH) and natural greigite (Fe_3S_4) and pyrrhotite (Fe_7S_8) to constrain interpretation of FORC diagrams from natural samples. Hematite and goethite have low spontaneous magnetizations and negligible magnetic interactions, while greigite and pyrrhotite have higher spontaneous magnetizations and can have strong magnetic interactions. The coercivity of hematite systematically increases with Al content only for samples produced using the same synthesis method, but it is variable for samples produced with different methods even for similar Al content. This precludes use of magnetic coercivity alone to quantify the Al content of natural hematites. Goethite has much higher coercivity than hematite for all measured samples. SD and superparamagnetic (SP) behavior is common in natural greigite samples, with peak coercivities ranging from $\sim$70 mT (SD) to zero (SP). This range overlaps with that of lower-coercivity minerals, which can make greigite identification ambiguous at room temperature. Fine-grained SD pyrrhotite has slightly higher coercivities than greigite, which progressively decreases with increasing grain size within the SD size range and overlaps the range for greigite. While FORC diagrams are useful for magnetic characterization, care is needed in interpretation because of overlaps in the broad range of magnetic properties, which result from variations in domain state, for any magnetic mineral with respect to other minerals.

Citation: Roberts, A. P., Q. Liu, C. J. Rowan, L. Chang, C. Carvallo, J. Torrent, and C.-S. Horng (2006), Characterization of hematite (α-Fe_2O_3), goethite (α-FeOOH), greigite (Fe_3S_4), and pyrrhotite (Fe_7S_8) using first-order reversal curve diagrams, *J. Geophys. Res.*, *111*, B12S35, doi:10.1029/2006JB004715.

1. Introduction

[2] First-order reversal curve (FORC) diagrams [*Pike et al.*, 1999; *Roberts et al.*, 2000] have become a standard tool for characterizing magnetic minerals, their domain states and the extent of magnetostatic interactions in paleomagnetism [e.g., *Weaver et al.*, 2002; *Rowan and Roberts*, 2006; *Tarduno et al.*, 2006; *Carvallo et al.*, 2006a], environmental magnetism [e.g., *van Oorschot et al.*, 2002; *Peck et al.*, 2004; *Muxworthy et al.*, 2005] and rock magnetism [e.g., *Muxworthy and Dunlop*, 2002; *Carvallo et al.*, 2003, 2004, 2006b; *Muxworthy et al.*, 2004]. Interpretation of FORC diagrams is derived from Néel's phenomenological interpretation of the Preisach diagram [*Preisach*, 1935; *Néel*, 1954], in which the FORC distribution $\rho(B_a, B_b)$ is the product of the coercivity distribution $g(B_c)$ and the interaction field distribution $f(B_i)$. The coercivity distribution for an assemblage of single domain (SD) particles is represented along the horizontal axis of a FORC diagram, while the interaction field distribution for the assemblage is portrayed along the vertical axis (Figures 1a and 1b). The framework for interpretation of FORC diagrams is described by *Pike et al.* [1999] and *Roberts et al.* [2000]; more complete descriptions are provided by *Pike et al.* [2001a] and *Muxworthy and Roberts* [2006]. This framework is supported by measurements of well characterized natural samples and numerical simulations [*Pike et al.*, 1999, 2001a, 2001b; *Roberts et al.*, 2000], as well as by micromagnetic models [*Carvallo et al.*, 2003, 2004; *Muxworthy et al.*, 2005; *Winklhofer and Zimanyi*, 2006]. Variations in domain state, magnetostatic interactions and thermal relaxation all produce distinct manifestations on FORC

[1]National Oceanography Centre, University of Southampton, Southampton, UK.
[2]Now at Institut de Minéralogie et de Physique de la Matière Condensée, Université Pierre et Marie Curie, Paris, France.
[3]Departamento de Ciencias y Recursos Agrícolas y Forestales, Universidad de Córdoba, Córdoba, Spain.
[4]Institute of Earth Sciences, Academia Sinica, Taipei, Taiwan.

0148-0227/06/2006JB004715$09.00

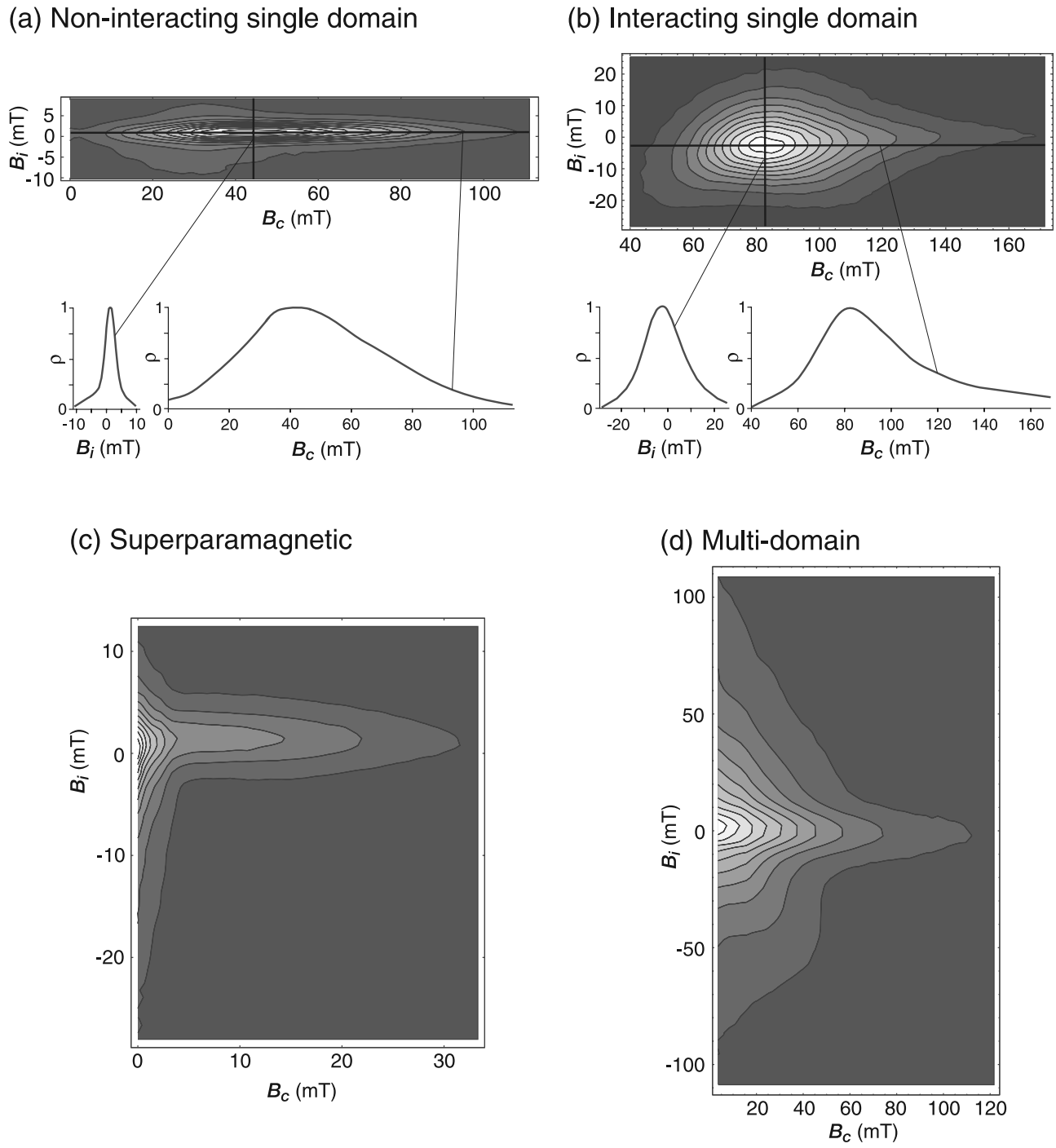

Figure 1. Illustration of the main types of magnetic behavior observed on FORC diagrams for (a) an assemblage of noninteracting SD particles (closed concentric contours with negligible vertical spread of the FORC distribution); (b) an assemblage of interacting SD particles (closed concentric contours with substantial vertical spread of the FORC distribution). The profiles through the peak of the normalized FORC density distributions (ρ) provide a measure of the interaction field (B_i) and coercivity (B_c) distributions. FORC diagrams for (c) an assemblage of particles close to the SP/SD threshold size (contours that intersect the B_i axis with low coercivities) and (d) an assemblage of MD particles (divergent contours that intersect the B_i axis, but with generally higher coercivities than for SP behavior). See *Pike et al.* [1999, 2001a, 2001b] and *Roberts et al.* [2000] for detailed explanations.

diagrams, which makes them useful for characterizing magnetic mineral assemblages in a range of applications in paleomagnetism, environmental magnetism and rock magnetism.

[3] To correctly interpret FORC diagrams from magnetically complex natural samples, it is crucial to have a detailed knowledge of the nature of FORC diagrams for a wide range of common magnetic minerals, including their

dependence on grain size and mineral stoichiometry (as well as other factors such as grain shape, internal stress, and the mode of occurrence of the grains). Despite widespread adoption of FORC diagrams in the paleomagnetic and rock magnetic community, most magnetic minerals remain largely uncharacterized using FORC diagrams. Magnetite (Fe_3O_4) is the only reasonably well characterized magnetic mineral, with detailed treatments of the SD [*Roberts et al.*, 2000; *Carvallo et al.*, 2003, 2004; *Newell*, 2005], pseudosingle-domain (PSD) [*Roberts et al.*, 2000; *Muxworthy and Dunlop*, 2002; *Carvallo et al.*, 2003], multidomain (MD) [*Roberts et al.*, 2000; *Pike et al.*, 2001a] and superparamagnetic (SP) [*Roberts et al.*, 2000; *Pike et al.*, 2001b] states. In this paper, we present FORC diagrams for well-characterized synthetic aluminous hematite (α-$Fe_{2-x}Al_xO_3$), synthetic aluminous goethite (α-(Fe,Al)OOH), natural greigite (Fe_3S_4) and natural monoclinic pyrrhotite (Fe_7S_8) samples to help constrain interpretation of FORC diagrams for natural samples containing these minerals.

2. Interpretation of FORC Diagrams

[4] FORC diagrams can enable discrimination between mixtures of grains with variable domain states and identification of the presence or absence of magnetostatic interactions because grains with different domain structures and interactions plot in different parts of the FORC diagram. SD particles produce FORC distributions with closed concentric contours about a central peak (Figures 1a and 1b). In the presence of strong magnetostatic interactions, a FORC distribution has much greater vertical spread (Figure 1b) compared to samples without significant interactions (Figure 1a). The interaction field distribution (Figures 1a and 1b) in SD particle systems can be quantified using measures of the vertical spread parallel to the B_i axis [e.g., *Pike et al.*, 1999; *Muxworthy and Dunlop*, 2002; *Carvallo et al.*, 2006a]. The location of the SD peak parallel to the B_c axis indicates the weighted average value of the microcoercivity distribution, while a cross section through the distribution along the B_c axis provides an indication of the distribution of particle microcoercivities (Figures 1a and 1b), although the presence of strong magnetic interactions can make it difficult to extract the true coercivity distribution [*Winklhofer and Zimanyi*, 2006].

[5] Thermal relaxation of fine SD grains gives rise to SP behavior, which shifts a SD FORC distribution to lower coercivities; the shift can be substantial and can make a distribution intersect the B_i axis (Figure 1c) [*Pike et al.*, 2001b]. The magnetization of ideal SP particles is, by definition, entirely reversible, which should therefore produce no manifestation on a FORC diagram. However, SP behavior strongly depends on measurement time. Particles with SP behavior will dominate a FORC diagram when the measurement time is comparable to the relaxation time of the majority of particles. FORC distributions of the type shown in Figure 1c are therefore indicative of magnetic assemblages with an abundance of particles close to the SD/SP threshold size [*Pike et al.*, 2001b].

[6] At the coarse end of the grain size spectrum, MD particles give rise to FORC distributions that strongly contrast with those from SD grains. *Pike et al.* [2001a] demonstrated that particles with strong domain wall pinning, such as transformer steel, produce FORC distributions with extremely low B_c values and nearly vertical contours. As MD particles decrease in size (Figure 1d), the contours of the FORC distribution become less steep, they intersect the B_i axis, and they extend to higher coercivities [*Roberts et al.*, 2000; *Pike et al.*, 2001a]. The inclined contours that intersect the B_i axis probably result from magnetic interactions among domain walls [*Dunlop et al.*, 1990]. The asymmetry of these FORC distributions and the generally higher coercivities of natural MD grains make it straightforward to discriminate MD from SP behavior on a FORC diagram (e.g., Figures 1c and 1d). Low-temperature FORC measurements also provide a powerful means of discriminating MD from SP behavior. At low temperatures, FORC distributions for SP particles will move to higher coercivities compared to room temperature measurements [*Pike et al.*, 2001b]; this will not occur for MD particles.

3. Methods

[7] Isothermal remanent magnetization (IRM) acquisition curves, magnetic hysteresis loops and FORC measurements were made using a Princeton Measurements Corporation vibrating sample magnetometer (VSM). The maximum applied field was 1 T; lower values were used as appropriate for samples that magnetically saturate at lower fields. A maximum applied field of 1 T will be insufficient to magnetically saturate high-coercivity minerals such as some hematites and goethite, which can remain unsaturated at fields >57 T [*Rochette et al.*, 2005]. Regardless, magnetic measurements in paleomagnetic, environmental magnetic and rock magnetic studies typically make use of instruments with similar maximum field capability to the VSM used in this study. It is important to understand the behavior of high-coercivity minerals using standard equipment and field settings despite the fact that the measurements do not represent saturation properties (which are rarely, if ever, measured for goethite). The approach used in this study is therefore valid, but it should be noted that the properties reported here for goethite are not saturation properties and that the applied fields should be carefully noted when comparing our data with results from other studies. Hysteresis parameters, including saturation remanent magnetization (M_{rs}), saturation magnetization (M_s), and B_c (coercive force) were determined after high-field slope correction. IRM acquisition curves were measured in a stepwise manner (with field increments of 5 mT) up to 1 T. To obtain the coercivity of remanence (B_{cr}), samples were remagnetized using back fields up to -1 T, after the IRM had been imparted up to +1 T. For each sample, 140 FORCs were measured with an averaging time of 250 ms and a wait time of 250 ms between successive measurements. FORC diagrams were either determined using the ''relaxed fit'' algorithm of *Pike et al.* [1999] (Figure 1 only) or the ''reversible ridge'' algorithm of *Pike* [2003] for all new data presented here (see *Muxworthy and Roberts* [2006] for a more detailed treatment of these methods, which only differ in the way that the FORC distribution is calculated near $B_c = 0$). In most cases, FORC diagrams were calculated using a smoothing factor (SF) of 5 (see *Roberts et al.* [2000] for details), although SF = 4 was usually used for strongly magnetic greigite and pyrrhotite samples, which were mea-

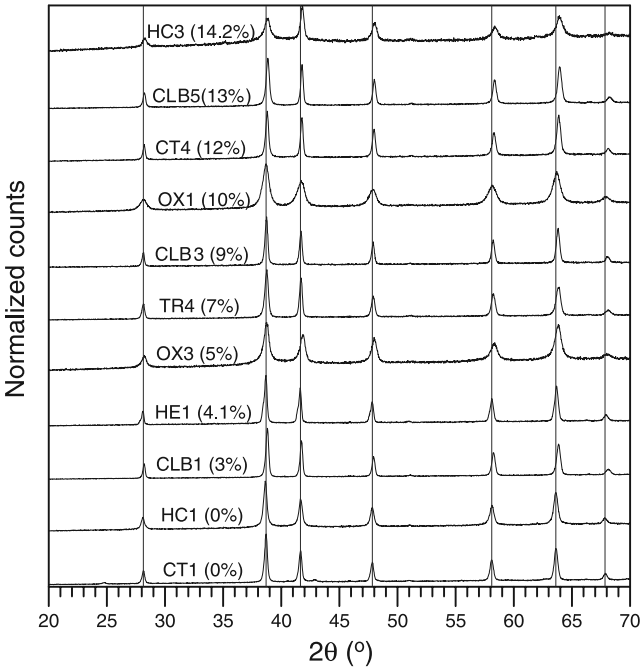

Figure 2. X-ray diffraction patterns that illustrate the purity of the studied aluminous hematite samples. The lines indicate the expected peaks for hematite (no other peaks are present). Note the progressive shift of peaks to higher 2θ values with increasing Al content.

sured in their natural state within bulk sediments unless stated otherwise. The synthetic hematite and goethite samples were prepared for measurement using ~10 mg powders that were dispersed and immobilized in a CaF_2 matrix.

[8] X-ray diffraction (XRD) spectra were measured using a Siemens D5005 X-ray diffractometer with a sealed tube, monochromatic Cu$K\alpha$ radiation at a scan speed of 0.005° 2θ s^{-1}. Scanning electron microscope (SEM) observations were made using a LEO 1450VP SEM, operated at 10–20 keV with an acceleration voltage of 17–20 pA. The synthetic samples were prepared for SEM observation by diluting a small amount of sample ($\ll$1 mg) in about 5 mL of distilled water, ultrasonically dispersing the sample, and then placing a drop of the suspension on a sample holder and allowing the sample to dry in air. A gold coating was used to increase the conductivity of samples for imaging.

4. Samples

4.1. Hematite

[9] Synthetic hematite samples with a wide range of isomorphically substituted aluminum (Al) contents were analyzed in this study. It is useful to consider not only pure hematite (α-Fe_2O_3), but also aluminous hematite (α-$Fe_{2-x}Al_xO_3$) because Al substitution is common in nature. For example, Al contents in the vicinity of 10% are observed in tropical acid soils, whereas values <7% are usually observed in soils from the Mediterranean region [*Torrent et al.*, 1980]. It is therefore important to understand the effects of Al substitution on commonly measured magnetic properties to test whether they can be used to detect variations in Al content, or, on the other hand, whether such variations complicate magnetic interpretation. These issues are particularly important in environmental magnetic studies. Several series of synthetic hematite samples, which were produced using different synthesis methods, were analyzed. Generally, all of the hematite samples were synthesized using neutralizing solutions of $Fe(NO_3)_3$ and $Al(NO_3)_3$ with KOH in different concentrations. The Al mol% was determined by analyzing Fe and Al by atomic absorption spectrophotometry after dissolving the samples in 11 M HCl. The maximum Al content is about 16%, which is the maximum observed both in synthetic and natural samples. The samples are from the same set that was described in detail by *Barrón et al.* [1988] and *Colombo et al.* [1994]. These samples are similar to soil hematites, in that they were grown from solution, although the synthetic hematites are on average larger than natural grains in soils.

[10] Details of the mineralogical characterization of the studied synthetic hematite samples are presented elsewhere [*Barrón et al.*, 1988; *Colombo et al.*, 1994], but we show relevant XRD (Figure 2) and SEM (Figure 3) analyses to establish sample purity and grain size. Representative XRD data for 11 of the analyzed samples demonstrate their purity, with only hematite peaks being evident. A progressive shift of peaks to higher 2θ values is evident with increasing Al substitution (Figure 2). XRD cannot detect impurities below the 2–5% level, so magnetically important impurities can possibly remain undetected using XRD. Such impurities were not detected in the original studies. In addition, the magnetization of magnetite is much higher than that of hematite, so slight contamination of magnetite will significantly increase the saturation magnetization. M_s values of our samples are consistent with published data, which excludes the possibility of slight contamination by magnetite. Electron micrographs of selected samples illustrate the range of grain sizes for these pure aluminous hematite samples (Figure 3). The hematite particles are flakey and generally range in size from 100 to 400 nm, although some particles are tens of nm across. The overall grain size is relatively uniform for the samples shown in Figure 3, and largely falls within the ~30 nm to ~15 μm size range expected for SD magnetic behavior in hematite [*Banerjee*, 1971]. *Dekkers and Linssen* [1989] suggested a lower maximum SD threshold size of ~1 μm for natural hematite of low-temperature origin. Even with this lower threshold size, the studied samples fall in the expected SD grain size range. SP behavior should also be expected for the smallest particles in these samples. Overall, however, this sample set should constrain the effects of Al substitution on the magnetic properties of hematite, with relatively little influence from grain size variations.

4.2. Goethite

[11] We made FORC measurements on a range of synthetic goethite samples with varying Al contents [α-(Fe,Al)OOH], which have been described and examined in detail by *Schulze and Schwertmann* [1984, 1987], *Torrent et al.* [1987], and *Liu et al.* [2004], and which have been subjected to detailed low-temperature magnetic analyses [*Liu et al.*, 2006]. The Al mol% ranges from 0 to 17.3%. XRD results, as summarized by *Liu et al.* [2006], demonstrate the presence of only goethite in the samples, which indicates that no alteration has occurred since they were

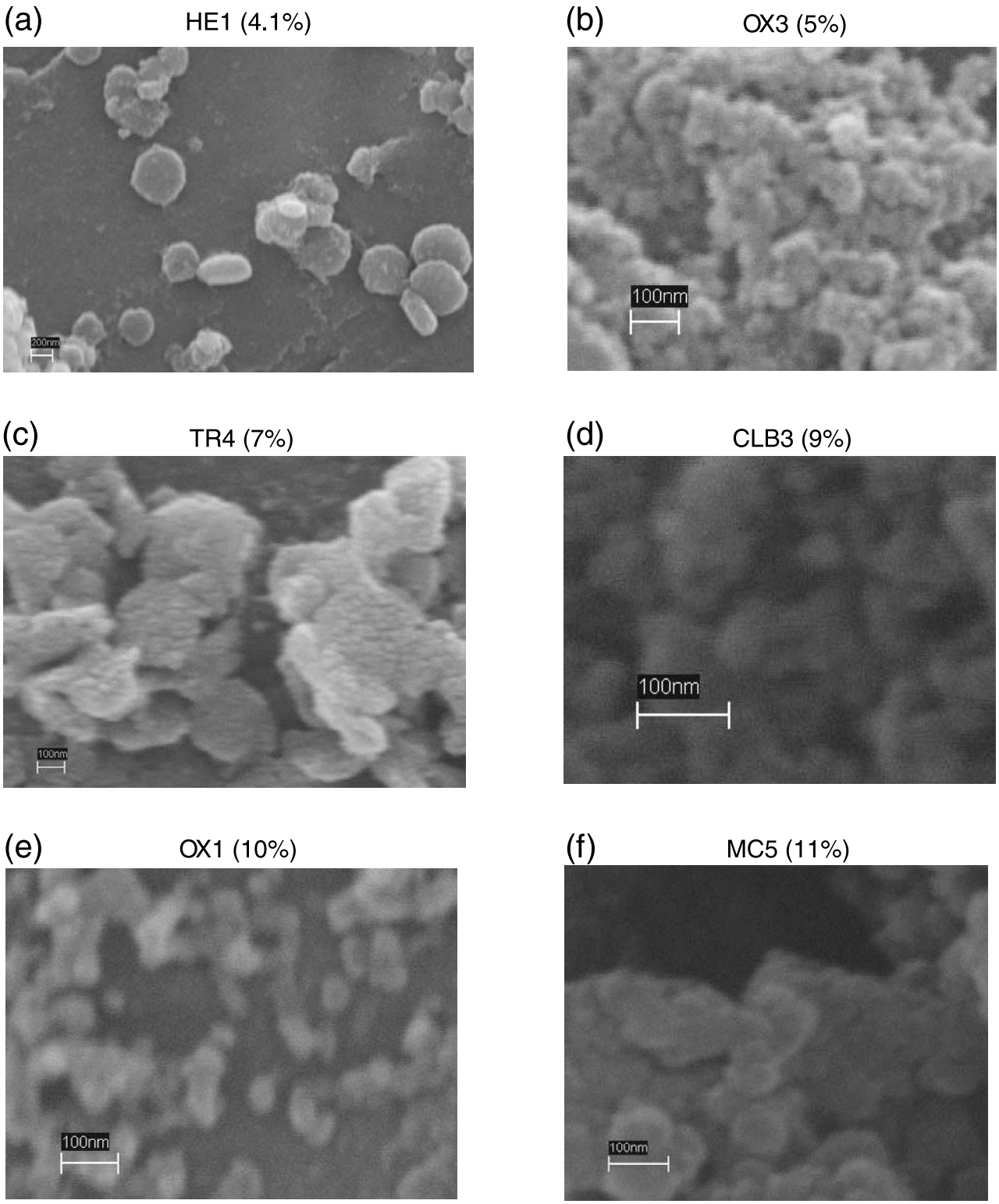

Figure 3. Backscattered electron images that illustrate the grain size and morphology of representative samples from the suite of studied aluminous hematite samples. Most of the grains fall in the expected size range ($\sim$30 nm to $\sim$1 μm) for SD hematite [*Banerjee*, 1971; *Dekkers and Linssen*, 1989].

originally synthesized. SEM observations indicate that the grain sizes of the studied Al goethite samples vary greatly, with pure goethite grains (0 mol% Al) having acicular shape with lengths of several hundreds of nm [*Liu et al.*, 2006]. With increasing Al substitution, the goethite grains generally become shorter. The samples have stable magnetizations at room temperature, with Néel temperatures between 311 and 380 K [*Liu et al.*, 2006]. FORC diagrams for these

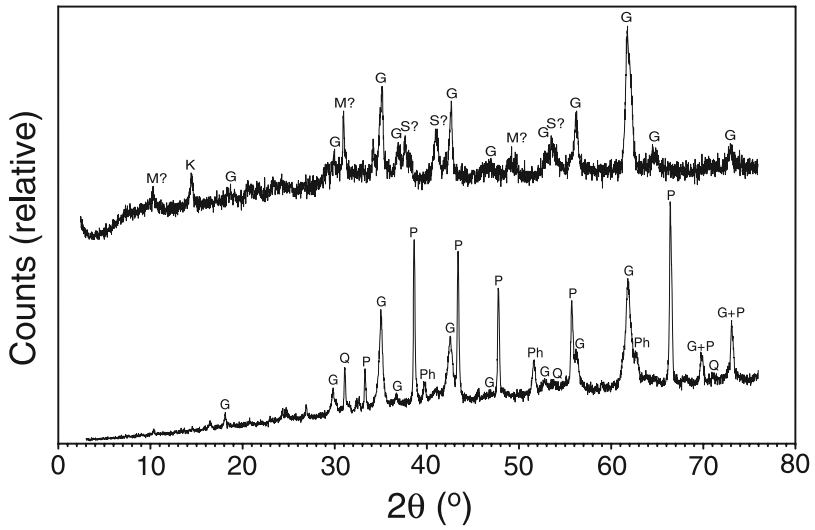

Figure 4. X-ray diffraction patterns for studied magnetic separates from greigite-bearing sediments from Bohemia, Czech Republic (top curve) [*Krs et al.*, 1990]; Valle Ricca, Italy (bottom curve) [*Florindo and Sagnotti*, 1995]. The samples are not as pure as the synthetic samples (compare Figure 2), but it is still clear that greigite is the main magnetic mineral present. Peaks are marked for each identified mineral (G, greigite; P, pyrite; Ph = hexagonal pyrrhotite; Q, quartz; K, kaolinite; S, smythite; M, marcasite). Smythite, which has similar chemistry and magnetic properties to greigite [*Hoffmann*, 1993], is present in the sample from the Czech Republic, and hexagonal pyrrhotite, which is not ferrimagnetic at room temperature, is present along with paramagnetic pyrite in the sample from Valle Ricca.

samples should therefore place useful constraints on interpretation of magnetic data from aluminous goethite-bearing natural samples.

4.3. Greigite

[12] We have produced FORC diagrams for well-characterized greigite-bearing samples from a wide range of localities worldwide. We present representative results from three groups of samples from this collection. First, we present results from bulk sediment samples containing SD greigite from southwestern Taiwan. Detailed mineralogical characterization of these samples has been presented by *Horng et al.* [1992, 1998] and *Jiang et al.* [2001]. Second, we show results of mixtures of SD and SP greigite for well-characterized samples from New Zealand [*Rowan and Roberts*, 2006]. Finally, we present results for three samples that have a range of magnetic properties, including a synthetic SP sample, a natural SD greigite sample (from a greigite nodule from the Valle Ricca section near Rome, Italy [*Florindo and Sagnotti*, 1995]), and a MD greigite sample (from coal-bearing lacustrine sediments from Bohemia, Czech Republic [*Krs et al.*, 1990; *Hoffmann*, 1992]). The synthetic sample was produced following the method of *Benning et al.* [2000], at 90°C, with ~0.13 M FeS, for 20 hours, at a final pH of 8.9. The presence of greigite in this sample was confirmed by X-ray absorption spectroscopy. XRD results for the SD and MD samples from Italy and the Czech Republic are shown in Figure 4; results of mineralogical characterization for other samples are not shown here since they are presented in the studies cited above. It is extremely difficult to obtain samples containing only greigite because pyrite usually grows simultaneously with greigite in synthetic samples [e.g., *Benning et al.*, 2000] and greigite co-occurs in intimate association with other iron sulphide phases or within phyllosilicate sheets in natural samples [e.g., *Jiang et al.*, 2001; *Roberts and Weaver*, 2005]. In addition to greigite, XRD results (Figure 4) contain evidence of pyrite and marcasite, which are paramagnetic at room temperature, and hexagonal pyrrhotite, which is antiferromagnetic at room temperature, and should therefore have no bearing on the FORC measurements. The sample from the Czech Republic also contains possible ferrimagnetic smythite (Fe_9S_{11}), which has similar magnetic characteristics to greigite [*Hoffmann*, 1993], so its presence in small quantities should not significantly affect our results.

4.4. Pyrrhotite

[13] FORC measurements were also made for bulk sediment samples containing SD monoclinic pyrrhotite from southwestern Taiwan (see *Horng et al.* [1992, 1998] for detailed mineralogical characterization of these samples). The pyrrhotite was originally interpreted to have authigenically formed during early diagenesis [e.g., *Horng et al.*, 1992, 1998; *Kao et al.*, 2004], but *Horng and Roberts* [2006] recently demonstrated from a detailed study of source rocks and of sediment transportation pathways that the pyrrhotite originates from metamorphic rocks in the Taiwan Central Range. XRD analyses of magnetic extracts from the studied Pleistocene sediments [*Horng et al.*, 1998] demonstrate that the pyrrhotite is the ferrimagnetic monoclinic species (the double peak at a 2θ angle of ~44° is diagnostic of Fe_7S_8) even though the morphology is (pseudo-) hexagonal (which makes it impossible to visually distinguish monoclinic from hexagonal pyrrhotite; *Horng and Roberts* [2006]). SEM observations indicate that the pyr-

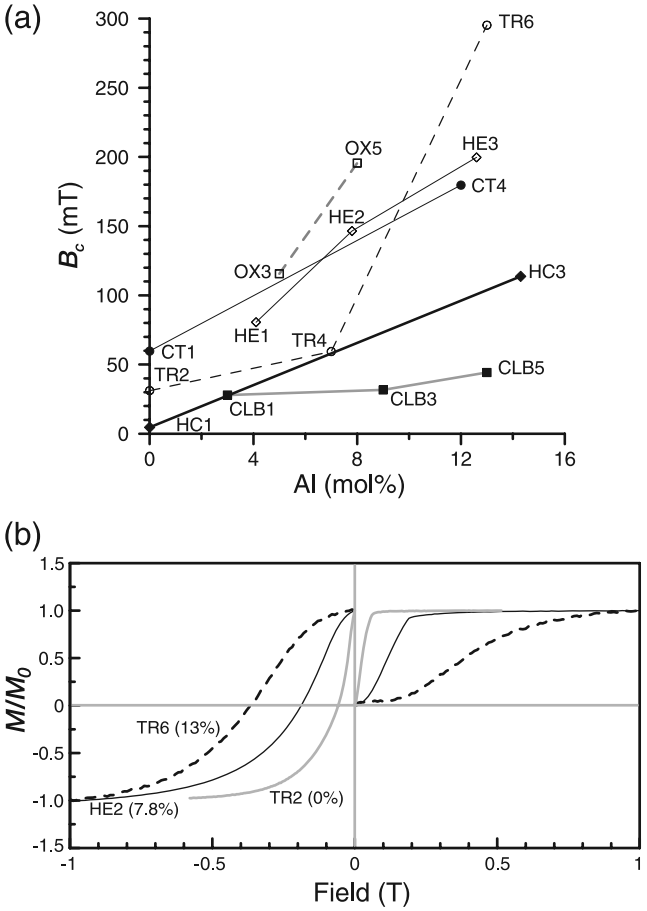

Figure 5. Measures of coercivity for Al-substituted hematite. (a) Bulk B_c (determined from hysteresis measurements) versus Al mol%. The lines join data for groups of samples synthesized with the same method. (b) IRM acquisition and back-field demagnetization curves for representative aluminous hematite samples. Coercivities increase with Al content for each sample series, but samples from different series can have markedly contrasting coercivities for the same Al content.

rhotite grains have regular morphologies, with widths of up to 10 μm across.

5. Results and Discussion

5.1. Hematite

[14] The magnetic properties of hematite and goethite are controlled by both grain size [*Dekkers*, 1989; *Dekkers and Linssen*, 1989; *de Boer and Dekkers*, 1998] and isomorphous cation substitutions [*Mathé et al.*, 1999; *Wells et al.*, 1999; *Liu et al.*, 2004]. It is therefore important to check the effects of both variables to test whether magnetic properties can unambiguously detect variations in grain size and stoichiometry. As stated above, the studied samples should dominantly lie within the SD grain size range (Figure 3), so our data should provide a test of the effects of isomorphous Al substitution on the magnetic properties of hematite.

[15] At first inspection, it is evident that the studied hematite samples with similar Al contents have strongly contrasting coercivities (Figure 5a). This clearly demonstrates that the products of the different hematite synthesis methods have highly variable magnetic properties. Nevertheless, closer inspection reveals some important trends. In particular, it is clear that, for the respective sample series from each synthesis method, there is a trend toward higher coercivities with higher Al substitution (Figure 5a). This is also generally evident in IRM acquisition curves (Figure 5b), where there is considerable variability in the fields at which saturation is achieved. For some samples (e.g., TR2, which has 0% Al), only a small proportion of the magnetization is not saturated at 300 mT, even though saturation is not achieved until 500 mT. Other samples with higher Al contents have much higher saturation fields (>800 mT). These results are important for interpretation of the "hard" IRM (HIRM) parameter or the S ratio [e.g., *Thompson and Oldfield*, 1986; *King and Channell*, 1991], which we will discuss in more detail elsewhere.

[16] For all of the analyzed aluminous hematite samples, the hysteresis loops are saturated or close to saturation at 1 T (Figures 6a–6j), which means that the coercivity distributions in our FORC measurements represent saturation properties. FORC diagrams for representative samples from 4 suites of synthetic aluminous hematites are shown in Figure 7. There is little vertical spread of the contours in the FORC diagrams, which indicates that magnetostatic interactions are negligible. The magnetizations of these samples are weak and a relatively high SF (5) was used to reduce noise. This will produce a vertical smearing of the contours, which is largely an artifact of the numerical procedure used to calculate the FORC distribution [*Pike et al.*, 1999], but smearing will also be more severe for high-coercivity minerals because larger field steps are needed to reach higher saturation fields using the same number of field measurements. Nevertheless, this spread is much less than that usually observed for SD greigite-bearing sediments [*Roberts et al.*, 2000] (see below), in which greigite commonly grows in closely packed aggregates [e.g., *Roberts and Weaver*, 2005]. The lack of magnetic interactions in these hematite samples is consistent with the observations of *Muxworthy et al.* [2005]. The other notable feature of the FORC diagrams for hematite (Figure 7) is the consistent trend to higher coercivities with increasing Al content. As shown in Figure 5a, the coercivities are not consistent for samples with similar Al values from different series, but the trend to higher coercivities with increasing Al content is evident within each series. In each case, the peak of the FORC distribution for nearly pure hematite can have surprisingly low coercivities (20–50 mT in Figures 7a and 7d), but in each case the distribution has a significant high-coercivity tail (>150 mT). Samples with intermediate to high Al contents in the CT, HE, and OX series (4.1–12.6% Al) all have much higher coercivities (Figures 7e–7j), which extend up to ~700 mT (Figure 7h).

[17] Overall, the FORC diagrams for aluminous hematite samples are indicative of noninteracting assemblages of SD grains with variable coercivities that generally increase with increasing Al contents. Any attempts to use these data to make inferences about the Al content, however, would not be appropriate because different synthesis methods produce a marked variation in magnetic properties for similar Al contents. Such inferences are only likely to be valid if all

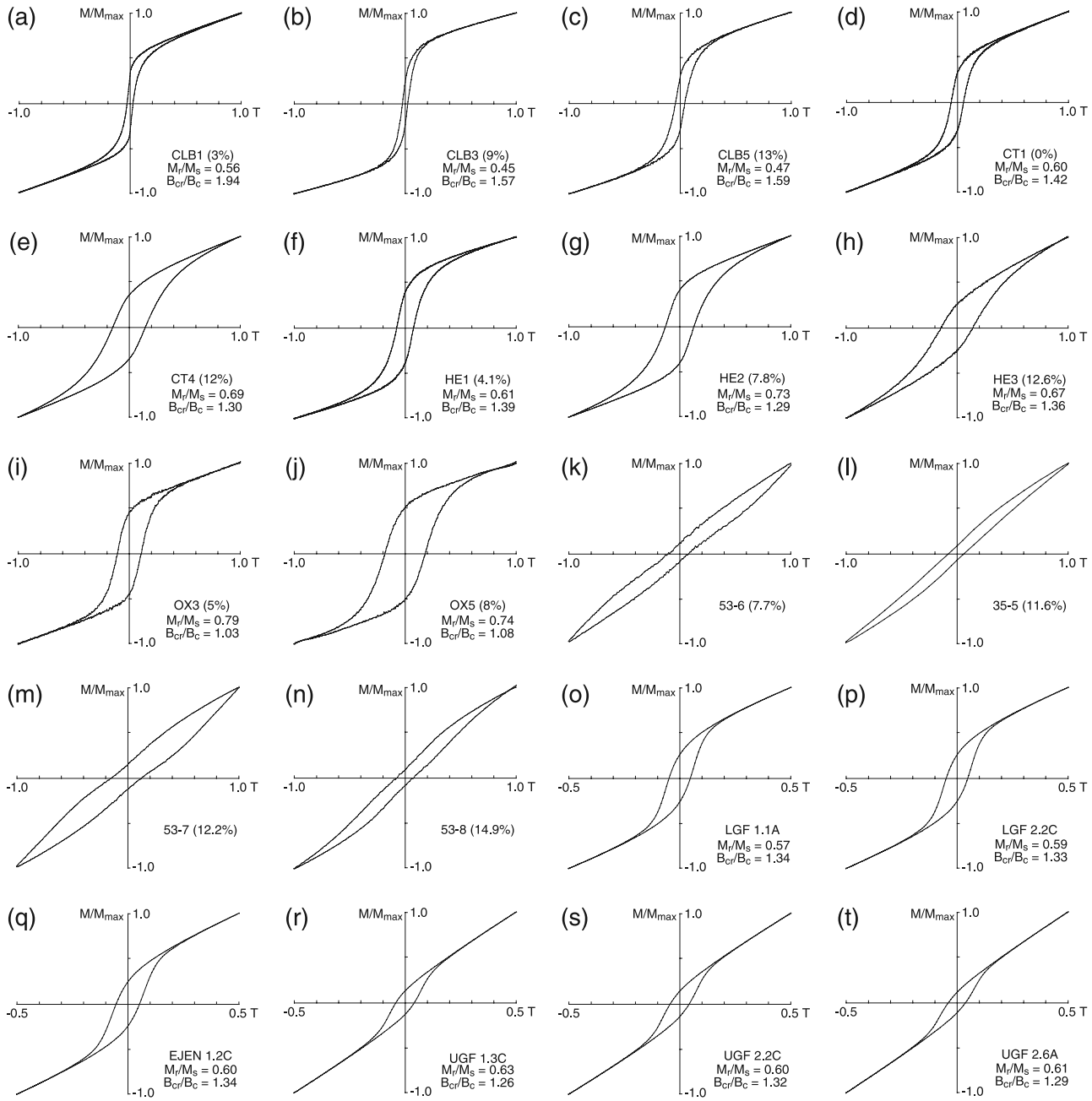

Figure 6. Hysteresis loops for (a–j) hematite, (k–n) goethite, (o–q) greigite and (r–t) pyrrhotite samples for which FORC diagrams are presented in this paper. The ratios of hysteresis parameters (M_r/M_s and B_{cr}/B_c) are consistent with the dominance of SD particles in each sample. The goethite samples are not close to magnetic saturation at 1 T, so no hysteresis ratios are reported. Some of the hematite samples are also not saturated, but these are closer to saturation, so hysteresis ratios are shown. Some loops are slightly wasp-waisted (e.g., Figure 6a), or are more strongly distorted (e.g., the goethite samples in Figures 6k–6n), which indicates a bimodal mixture of coercivities [*Roberts et al.*, 1995]. The percentages in parentheses refer to mol % A1 for the aluminous hematite and goethite samples.

aluminous hematite in an environment had similar genesis. Isomorphous substitutions of Al have probably caused increased imperfections and nonuniformity within the crystal structure of the hematite grains, which has contributed to the increased magnetic hardness with increased Al content [*Liu et al.*, 2006]. As indicated by SEM images (Figure 3), some extremely small grains are present in the hematite samples. The fact that a significant proportion of the grains are in the SP state is demonstrated by the secondary peak at the origin of some of the FORC diagrams (e.g., Figures 7a–7d). These samples also have the lowest-coercivity distributions of the studied samples, so it is not surprising that some of the grains are small enough to have undergone thermal relaxation. Values for the peak of the FORC distribution are plotted versus B_c values obtained from the respective hysteresis loops in Figure 7k. The two methods for

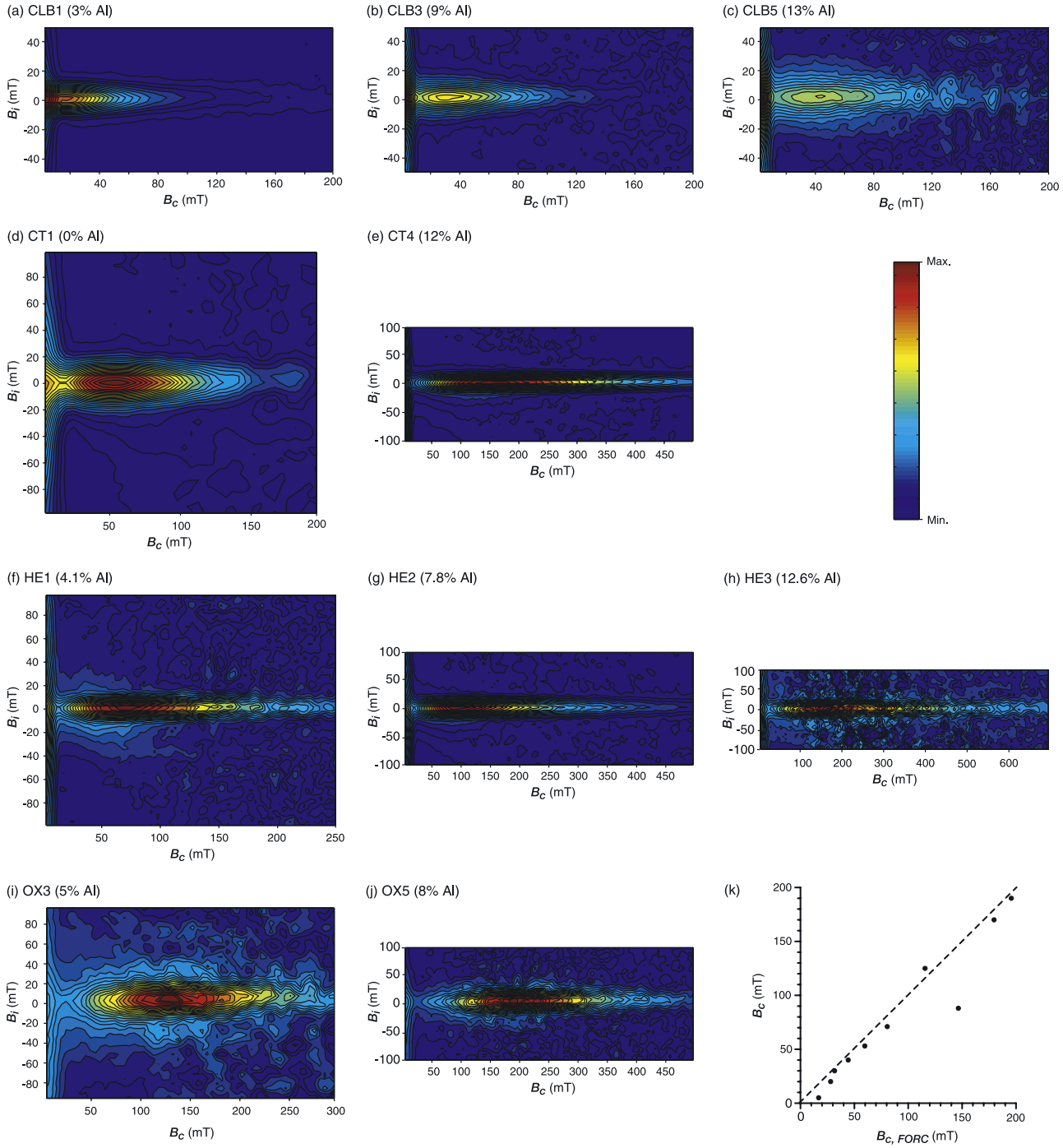

Figure 7. FORC diagrams for synthetic aluminous hematite samples (SF = 5 in all cases), where each horizontal row of diagrams represents a different sample series (produced with different synthesis methods). The samples are (a) CLB1 (3 mol% Al); (b) CLB3 (9 mol% Al); (c) CLB5 (13 mol% Al); (d) CT1 (0 mol% Al); (e) CT4 (12 mol% Al); (f) HE1 (4.1 mol% Al); (g) HE2 (7.8 mol% Al); (h) HE3 (12.6 mol% Al); (i) OX3 (5 mol% Al); and (j) OX5 (8 mol% Al). Interactions are negligible, and the coercivities increase with Al content for each sample series, although hematite samples with equivalent Al contents from different sample series can have markedly different magnetic properties. The variable size of the FORC diagrams reflects the need to maintain a consistent aspect ratio so that the vertical and horizontal scales are the same for each diagram. The relative scale on the right-hand side of the figure is the same for all successive figures and is not reproduced in each figure. (k) Plot of the bulk coercivity (B_c) obtained from the corresponding hysteresis loop versus the coercivity indicated by the peak of the FORC distribution ($B_{c,\ \mathrm{FORC}}$) for the 10 measured hematite samples.

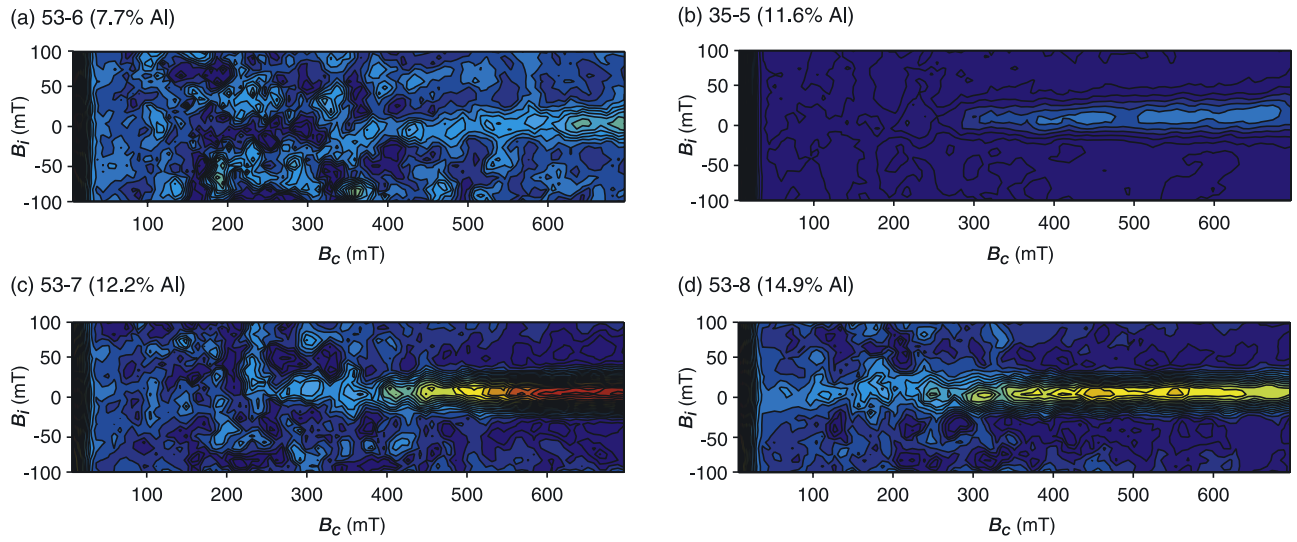

Figure 8. FORC diagrams for synthetic aluminous goethite samples (SF = 5 in all cases): (a) 53–6 (7.7 mol % Al); (b) 35–5 (11.6 mol % Al); (c) 53–7 (12.2 mol% Al); and (d) 53–8 (14.9 mol % Al). The high level of noise in the FORC diagrams is a result of the low M_s of the goethite samples.

determining B_c provide similar estimates, which plot close to a line with 1:1 slope. Estimates of B_c from hysteresis loops are generally higher than those obtained from FORC diagrams, probably because the high-coercivity part of the hematite assemblage will contribute more to the bulk measurement than to the peak of the FORC distribution. Regardless, this is a useful verification of the general equivalence of the peak value of the FORC distribution with the bulk coercive force, B_c, which we expect to be valid as long as the hysteresis loop is not distorted [cf. *Roberts et al.*, 1995].

[18] Two recent studies have tested the ability of FORC diagrams to detect mixtures of minerals with weak spontaneous magnetizations (e.g., hematite and goethite) with more strongly magnetic minerals such as magnetite [*Muxworthy et al.*, 2005; *Carvallo et al.*, 2006b]. *Muxworthy et al.* [2005] reported that minerals with high spontaneous magnetizations will dominate the signal generated by minerals with weak spontaneous magnetizations even when the strongly magnetic phase has concentrations of only ~3%. Nevertheless, the high-coercivity (low spontaneous magnetization) component is still evident even when magnetite has concentrations of ~19%. Thus, despite limitations of FORC diagrams when dealing with mixtures of minerals with strongly contrasting spontaneous magnetizations, *Muxworthy et al.* [2005] noted that they enable better discrimination of components than standard hysteresis measurements.

5.2. Goethite

[19] As would be expected, the hysteresis loops for the studied synthetic goethite samples are not saturated at the maximum applied field of 1 T (Figures 6k–6n). Even so, the lowest coercivities observed in the FORC distributions are ~300 mT, while the peaks of the microcoercivity distributions exceed 700 mT (Figure 8). These coercivities are far higher than those of the studied hematite samples (Figure 7). As is the case for hematite, magnetic interactions are negligible for the studied goethite samples, which is a result of the low M_s of goethite. Unlike hematite, it is difficult to make inferences about the effects of Al substitution on FORC distributions with the present data set because the maximum applied fields are too low to enable observation of the main part of the coercivity distribution and therefore to observe trends with varying Al content.

[20] Few FORC diagrams have been reported in the literature for goethite. *Roberts et al.* [2000] published FORC diagrams for a goethite-bearing brick from a 14th century Bulgarian church. Magnetic interactions were negligible in this sample and the peak of the FORC distribution had a coercivity of ~530 mT. This result is consistent with those presented in Figure 8 and with the known magnetic properties of goethite [e.g., *Dekkers*, 1989]. *Muxworthy et al.* [2005] presented results from a goethite-bearing sample (64%) with significant hematite impurities (36%), which, because of the impurities, is not comparable to our FORC diagrams.

[21] The key point concerning goethite from this study is that it should have extremely high coercivities in FORC diagrams even with maximum applied fields of 1 T. It should be noted, however, that a pure goethite sample, which was the sample that *Rochette et al.* [2005] could not saturate even in applied fields of 57 T, did not yield a FORC distribution at maximum applied fields of 1 T in this study because this field was too weak to magnetize the sample. Lack of indication of a high-coercivity contribution to a FORC distribution is therefore not diagnostic of the absence of goethite. This observation complicates interpretation of FORC diagrams for goethite-bearing samples. It should also be noted that these goethite samples have unblocking temperatures (T_b) above room temperature. With increasing Al mol%, T_b gradually approaches room temperature, and the corresponding coercivity significantly decreases [*Liu et al.*, 2004]. Knowledge of the domain state of goethite particles in natural samples is therefore critical for assessing its contribution to bulk magnetic properties. It is clear that further work at high fields is necessary to better characterize aluminous goethite using FORC diagrams.

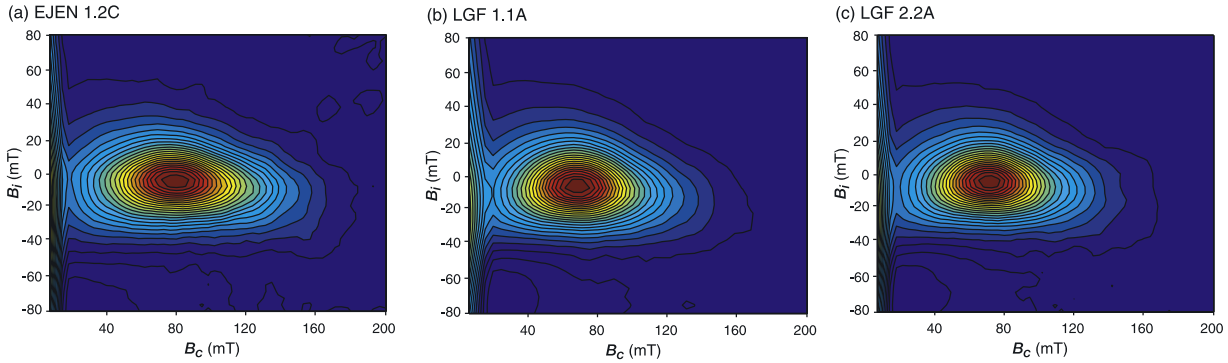

Figure 9. FORC diagrams for greigite-bearing sediments (SF = 4 in all cases) from southwestern Taiwan (EJEN, lower Pliocene portion of the Erhjen-chi section [*Jiang et al.*, 2001]; LGF, Lower Gutingkeng Formation (Pleistocene), also from the Erhjen-chi section [*Horng et al.*, 1992]). The FORC diagrams indicate the presence of strong magnetic interactions with relatively high, but variable, peak coercivities (60–75 mT).

5.3. Greigite

[22] *Roberts* [1995] demonstrated that many natural greigite samples have dominantly SD-like magnetic properties. Greigite-bearing samples from southwestern Taiwan with classic SD-like properties have FORC distributions with concentric contours (Figure 9) [see also *Roberts et al.*, 2000; *Sagnotti et al.*, 2005; *Rowan and Roberts*, 2006]. This observation confirms the interpretation that the observed SD-like properties of greigite [cf. *Roberts*, 1995] represent genuine SD magnetic behavior. In addition to having characteristic concentric contours, these FORC distributions have a negative region in the lower left-hand part of the FORC diagram (Figure 9). Many FORC diagrams are scaled in a manner such that this part of the distribution is not shown, but, as demonstrated by *Newell* [2005], this negative part of the FORC distribution is a result of the magnetic response of a SD particle assemblage (see *Muxworthy and Roberts* [2006] for a detailed explanation). The concentric contours also have considerable vertical spread (Figure 9), which is indicative of magnetostatic interactions [*Pike et al.*, 1999; *Roberts et al.*, 2000]. SEM images consistently indicate that sedimentary greigite authigenically grows in clumps, usually with the particles in contact with each other [e.g., *Jiang et al.*, 2001; *Roberts and Weaver*, 2005; *Sagnotti et al.*, 2005; *Rowan and Roberts*, 2006]. Micromagnetic models confirm that such small interparticle distances will result in substantial magnetostatic interactions and vertical spread of contours on FORC diagrams [*Carvallo et al.*, 2003; *Muxworthy et al.*, 2004].

[23] In addition to these classic SD properties, greigite-bearing samples from eastern New Zealand [*Rowan and Roberts*, 2006] dominantly yield FORC diagrams that are characteristic of thermally relaxed SP particles (e.g., samples TI02A and TC23A in Figure 10) [cf. *Pike et al.*, 2001b]. Detailed SEM investigations demonstrate the presence of substantial concentrations of greigite in the studied samples [*Rowan and Roberts*, 2006]. Authigenic mineral growth involves a progression from nothing to a finite size. It is, therefore, unsurprising that a substantial volume of greigite within sediments must be extremely fine grained. Plotting data for all samples from the New Zealand study of *Rowan and Roberts* [2006] on a Day diagram [*Day et al.*, 1977] demonstrates that they fall on a mixing line between SD and SP end-members (Figure 10) [cf. *Dunlop*, 2002], and that SP behavior is much more common in the studied sediments than the thermally stable SD behavior emphasized by *Roberts* [1995]. While the Day diagram and the 5 and 10 nm mixing trends of *Dunlop* [2002] are strictly only applicable to (titano-) magnetite, and are not rigorously applicable to greigite, which has magnetocrystalline anisotropy rather than uniaxial anisotropy [*Roberts*, 1995], it is useful to plot the data for greigite against the trends expected for magnetite in Figure 10 for the sake of reference. Recognition of the potential dominance of SP behavior in greigite in some settings in addition to SD greigite provides a completely new view of the magnetic properties of sedimentary greigite and substantially increases the range of magnetic properties, and therefore the range of potential geological occurrences, of greigite. It also demonstrates that greigite can display magnetic properties that are less easy to distinguish from those of other low-coercivity minerals such as magnetite.

[24] Extremes from the range of FORC diagrams that we have measured for greigite-bearing samples are shown in Figure 11. Synthetic greigite samples are often very fine grained (see the electron micrographs of *Dekkers and Schoonen* [1996] and *Benning et al.* [2000]). Considerable magnetic unblocking during warming of an IRM for many synthetic greigite samples from low temperatures confirms the presence of substantial populations of SP grains in such samples [e.g., *Roberts*, 1995; *Dekkers et al.*, 2000]. It is therefore unsurprising that SP behavior dominates the FORC diagram for a synthetic sample (Figure 11a) that was stored under anoxic conditions and that was measured shortly after synthesis. This FORC diagram is similar to, but less noisy than, those obtained for lower concentrations of SP greigite particles in sediments from New Zealand (Figure 10). A FORC diagram for a "normal" SD sample from Valle Ricca, Italy [*Florindo and Sagnotti*, 1995], is shown in Figure 11b (see Figure 4 for corresponding XRD data). The coarsest grained greigite known in the literature is from Miocene coal-bearing lacustrine sediments from the Czech Republic [*Krs et al.*, 1990]. *Hoffmann* [1992] demonstrated, using the magneto-optical Kerr effect, that grei-

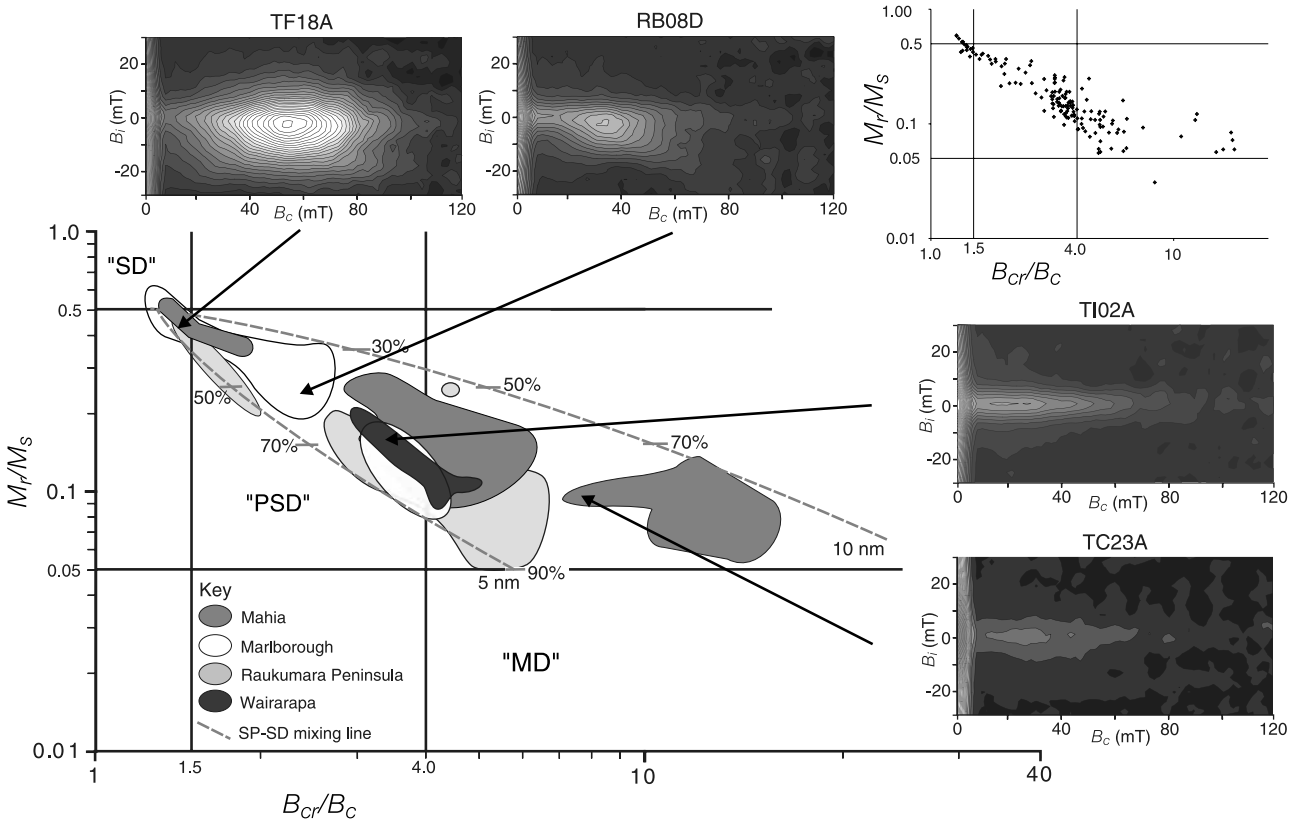

Figure 10. Plot of M_r/M_s versus B_{cr}/B_c [cf. *Day et al.*, 1977] for greigite-bearing sediment samples from eastern New Zealand [see *Rowan and Roberts*, 2006], with illustration of the relationship between hysteresis parameters and FORC distributions (SF = 5) of selected samples. The FORC distribution for sample TF18A is indicative of a population of SD greigite grains with strong magnetostatic interactions. Sample RB08D also contains a population of SD greigite, with decreased interactions and a coercivity distribution that is shifted toward the origin by thermal relaxation. The SD peak gets proportionally smaller and also shifts toward the origin of the FORC diagrams, due to proportionally increased thermal relaxation, in samples TI02A and TC23A. The smaller Day plot on the top right-hand side of the figure illustrates the individual data that are summarized in the main figure. Theoretical curves for mixtures of SD and SP (titano)magnetite [*Dunlop*, 2002] are plotted for 5 nm and 10 nm SP grains (% refers to % SP grains), although the assumption of a constant SP grain size is probably not valid in this case. Compared to the SD properties of sample TF18A, most samples contain large proportions of SP greigite.

gite grains from these deposits contain domain walls and that the SD/MD threshold size lies between 0.7 and 0.8 μm. The FORC diagram shown in Figure 11c contains evidence for the coarsest greigite that we have observed. It contains a typical SD peak for greigite at ~60 mT, but, at lower coercivities, the FORC distribution is inconsistent with that expected for a SD distribution because the inner contours have greater vertical spread and the outermost contours diverge rather than converge. We interpret this FORC diagram as containing evidence of both SD and MD grains. Further work is necessary to extract MD grains from this sample to obtain a more pure MD FORC distribution. Overall, the data shown in Figure 11 illustrate the range of domain states currently characterized with FORC diagrams for greigite.

5.4. Pyrrhotite

[25] FORC diagrams for sediment samples containing detrital monoclinic pyrrhotite grains are shown in Figure 12. All of the analyzed samples produce FORC distributions that are characteristic of magnetically interacting SD particle distributions, and are difficult to distinguish from those for greigite (Figure 9), as shown using vertical and horizontal profiles through the peaks of the FORC distributions (Figure 13). The greigite (Lower Gutingkeng Formation; LGF) and pyrrhotite (Upper Gutingkeng Formation; UGF) samples used for Figures 9 and 12 are from different parts of the Erhjen-chi section, southwestern Taiwan [*Horng et al.*, 1992]. The greigite-bearing EJEN samples are from the lower Pliocene portion of the LGF in the Erhjen-chi section [*Jiang et al.*, 2001]. The only observable difference between the FORC diagrams for greigite and pyrrhotite is the coercivity indicated by the peak of the FORC distributions. For greigite, the peaks are more variable (60–75 mT) and overlap with the lower range of values observed for the pyrrhotite samples (70–85 mT; Figure 13a). There is no discernible difference in the distribution of interaction field strengths (Figure 13b). The number of samples that we have analyzed from southwestern Taiwan (pyrrhotite, n = 10; greigite, n = 15) is too small to confidently assert whether

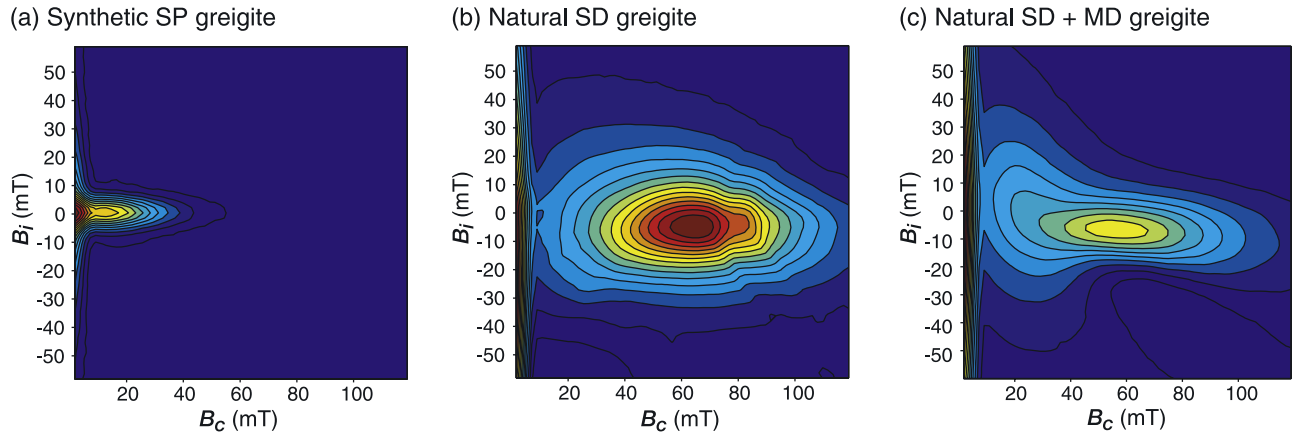

Figure 11. FORC diagrams for a range of greigite-bearing samples. (a) A synthetic greigite sample with dominantly SP behavior; (b) a typical natural greigite sample with SD magnetic properties from a greigite-bearing nodule (see XRD pattern in Figure 4) from the Valle Ricca section, near Rome, Italy [*Florindo and Sagnotti*, 1995]; (c) a natural greigite sample containing a mixture of SD (concentric contours) and MD (divergent contours) grains (see XRD pattern in Figure 4) from Bohemia, Czech Republic [*Krs et al.*, 1990].

the observed coercivity difference could be used to discriminate SD greigite from SD pyrrhotite, although there is a clear overlap in coercivities for the two minerals in our measurements (Figure 13a). Analysis of a wider range of pyrrhotite samples is needed to address this question.

[26] FORC diagrams have also been reported for SD pyrrhotite by *Weaver et al.* [2002] and *Wehland et al.* [2005]. The FORC diagrams that *Weaver et al.* [2002] obtained for pyrrhotite indicated the presence of strong magnetic interactions, which is consistent with SEM observations of interlocking plates of pyrrhotite that grew during acquisition of a synfolding magnetization. Furthermore, the peak of the FORC distributions was lower (~60 mT) than those reported in Figure 12, which indicates a further overlap with the coercivity range documented in Figure 9 for thermally stable SD greigite. This indicates that the peak coercivity can be highly variable, and that it can be difficult to discriminate greigite from pyrrhotite using FORC diagrams alone.

[27] The most comprehensive study of FORC diagrams for pyrrhotite is that of *Wehland et al.* [2005] who analyzed different grain size fractions from the crushed, equidimensional, natural pyrrhotite samples of *Dekkers* [1988] that originated from a hydrothermal ore deposit in Tuscany, Italy. They also analyzed pyrrhotite-bearing samples from metamorphic limestones. *Wehland et al.* [2005] reported FORC distributions that are characteristic of SD particle assemblages for grain sizes of <5 μm up to 30–40 μm. Grains in the 30–40 μm size range, which were taken to mark the upper limit of the PSD size range [*Soffel*, 1981], still have clear SD behavior in the FORC diagram shown by *Wehland et al.* [2005]. The coercivities indicated by the SD peaks in the FORC distributions for the sized pyrrhotite samples progressively decrease with increasing grain size from ~75 mT for the <5 μm fraction, to ~55 mT for the 5–10 μm fraction, to ~45 mT for the 10–15 μm fraction, to ~30 mT for the 15–20 μm fraction, to ~25 mT for the 20–25 μm fraction, and to ~15 mT for the 30–40 μm fraction. All of these samples contain evidence of magnetic inter-

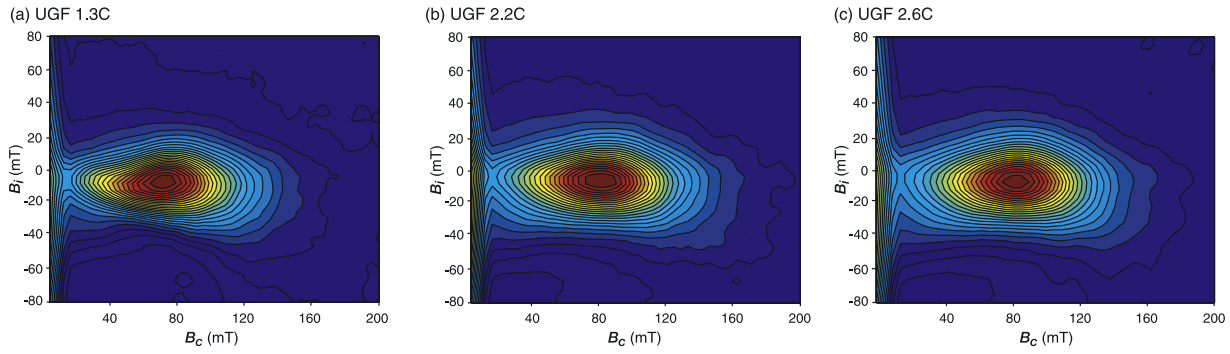

Figure 12. FORC diagrams for Pleistocene pyrrhotite-bearing sediments (SF = 4 in all cases) from southwestern Taiwan (UGF, Upper Gutingkeng Formation, from the Erhjen-chi section [*Horng et al.*, 1992]). The sedimentary pyrrhotite grains have a detrital origin and are sourced from metamorphic rocks in the Taiwan Central Range [*Horng and Roberts*, 2006]. The FORC diagrams indicate the presence of strong magnetic interactions with relatively high peak coercivities (70–85 mT).

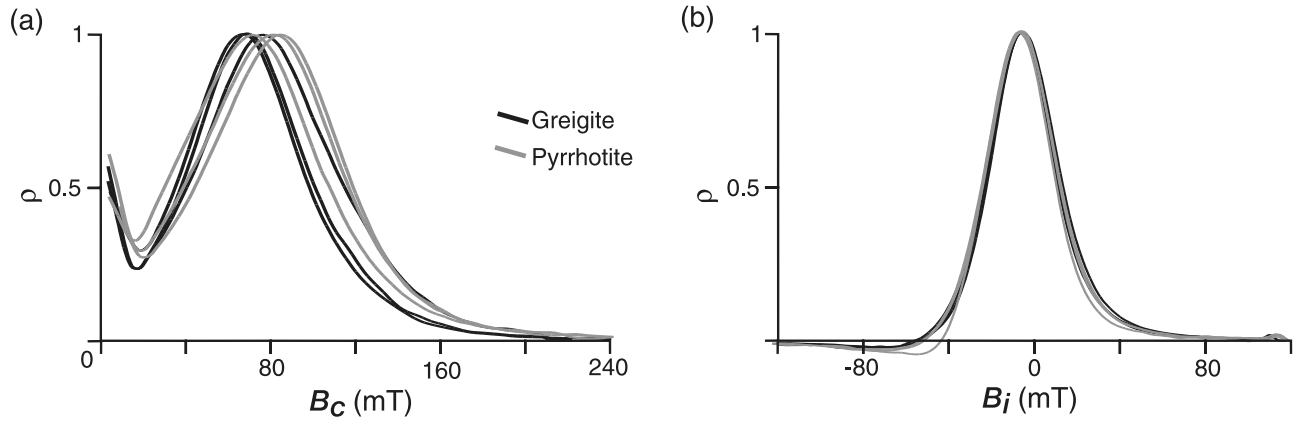

Figure 13. Profiles of the coercivity (B_c) and interaction field (B_i) distributions through the peak of the FORC distributions (ρ) for the greigite and pyrrhotite samples shown in Figures 9 and 12, respectively. The coercivity distributions overlap for the two minerals, while the interaction field distributions are indistinguishable.

actions that are slightly less than or similar to those shown in Figure 12, which *Wehland et al.* [2005] attributed to the existence of microtwins in the pyrrhotite grains that resulted from hammering during preparation of the samples into distinct size fractions. A range of samples with size ranges of 40–55 μm to 150–250 μm yielded FORC diagrams that progressively indicate PSD to large MD behavior.

[28] Our results in Figure 12 are for pyrrhotite grains that range up to about 10 μm in size [*Horng et al.*, 1998; *Horng and Roberts*, 2006]. The peak coercivity values that we observe in Figure 12 are consistent with those of the finest (<5 μm) grain size fraction measured by *Wehland et al.* [2005]. While this is reassuringly consistent, results from metamorphic limestones provide more variable results [*Wehland et al.*, 2005]. The metamorphic rocks produce FORC distributions with negligible vertical spread and much higher SD coercivities ranging from peak values of ~125 mT to maximum values of >400 mT. Such marked differences in observed magnetic properties (interactions and coercivities) of crushed pyrrhotite grains compared to those of metamorphic rocks raises important questions that require further systematic work on pyrrhotite to determine the interplay of magnetic properties with stress, grain size, and preferred orientation of minerals in metamorphic rocks in relation to the applied field direction.

6. Conclusions

[29] FORC diagrams provide detailed information about the coercivity and interaction field distribution of magnetic particles in samples, which represents a substantial advantage over most rock magnetic techniques (which usually provide a bulk measurement that represents a weighted sum of the magnetic components in the sample). Nevertheless, our results for several magnetic minerals (hematite, goethite, greigite and pyrrhotite) suggest that considerable care is needed when interpreting FORC diagrams. The aluminous goethite samples that we have analyzed (with Al content ranging from 7.7 to 14.9 mol%) have by far the highest coercivities (>700 mT) that are unlikely to be confused with other minerals. Nevertheless, thermal relaxation will occur within fine particles for all magnetic minerals, which will shift the FORC distributions to lower-coercivity ranges, which can potentially complicate interpretation of FORC diagrams. For goethite, there is an additional complication: high Al contents (>14.9 mol%) will cause paramagnetic behavior at room temperature because T_b < 300 K. The magnetic properties of hematite are also complicated by Al substitution. If all aluminous hematite grains grow via the same process within an environment, one would expect a general increase in coercivity with increasing Al content. However, the coercivities of samples produced via different processes will be variable for similar Al content. The presence of hematite grains with different provenance (e.g., detrital and authigenic) would therefore compromise efforts to infer the Al content of aluminous hematites from their magnetic properties alone. Hematite and goethite both have low spontaneous magnetizations and magnetostatic interactions are negligible in all studied samples.

[30] SD greigite and pyrrhotite (both from sediments) have similar coercivities and interaction field strengths, which makes it difficult to discriminate the two minerals on the basis of FORC diagrams alone, although SD pyrrhotite in metamorphic rocks can have much higher coercivities than greigite. Thermal relaxation in greigite and increasing grain size within the SD size range for crushed natural pyrrhotites both produce decreased coercivities, which also complicates discrimination of these minerals.

[31] The wide range of magnetic properties that is inherently produced by variations in domain state and thermal relaxation for different magnetic minerals causes an overlap in almost all magnetic properties for many minerals. This makes detailed characterization of the magnetic properties of magnetic minerals impossible with only a single method, including FORC diagrams. While FORC diagrams are highly useful for determining the distribution of interaction field strengths and coercivities, a range of methods should always be applied to magnetically characterize samples in detail.

[32] **Acknowledgments.** Qingsong Liu and Claire Carvallo were supported by Marie Curie fellowships, funded by the European Commission (proposal 7555 and EC contract MCIF-CT-2004-0107843, respectively),

Liao Chang is supported by the U.K. Natural Environment Research Council, and the contribution of José Torrent was supported by the Spanish Ministerio de Ciencia y Tecnología, Project AGL2003–01510. All new FORC data presented here were processed using the software produced by Michael Winklhofer. We thank Fabio Florindo, Liane Benning, and Petr Pruner for their help in supplying the greigite samples used in Figure 11 and Alexei Smirnov (Associate Editor), Mark Dekkers, Ramon Egli, and Michael Winklhofer for constructive comments that helped to improve the paper.

References

Banerjee, S. K. (1971), New grain size limits for palaeomagnetic stability in hematite, *Nature Phys. Sci.*, *232*, 15–16.

Barrón, V., M. Herruzo, and J. Torrent (1988), Phosphate adsorption by aluminous hematites of different shapes, *Soil Sci. Soc. Am. J.*, *52*, 647–651.

Benning, L. G., R. T. Wilkin, and H. L. Barnes (2000), Reaction pathways in the Fe-S system below 100°C, *Chem. Geol.*, *167*, 25–51.

Carvallo, C., A. R. Muxworthy, D. J. Dunlop, and W. Williams (2003), Micromagnetic modeling of first-order reversal curve (FORC) diagrams for single-domain and pseudo-single-domain magnetite, *Earth Planet. Sci. Lett.*, *213*, 375–390.

Carvallo, C., Ö. Özdemir, and D. J. Dunlop (2004), First-order reversal curve (FORC) diagrams of elongated single-domain grains at high and low temperatures, *J. Geophys. Res.*, *109*, B04105, doi:10.1029/2003JB002539.

Carvallo, C., A. P. Roberts, R. Leonhardt, C. Laj, C. Kissel, M. Perrin, and P. Camps (2006a), Increasing the efficiency of paleointensity analyses by selection of samples using first-order reversal curve (FORC) diagrams, *J. Geophys. Res.*, doi:10.1029/2005JB004126, in press.

Carvallo, C., A. R. Muxworthy, and D. J. Dunlop (2006b), First-order reversal curve (FORC) diagrams of magnetic mixtures: Micromagnetic models and measurements, *Phys. Earth Planet. Inter.*, *154*, 308–322.

Colombo, C., V. Barrón, and J. Torrent (1994), Phosphate adsorption and desorption in relation to morphology and crystal properties of synthetic hematites, *Geochim. Cosmochim. Acta*, *58*, 1261–1269.

Day, R., M. Fuller, and V. A. Schmidt (1977), Hysteresis properties of titanomagnetites: Grain size and composition dependence, *Phys. Earth Planet. Inter.*, *13*, 260–267.

de Boer, C. B., and M. J. Dekkers (1998), Thermomagnetic behaviour of haematite and goethite as a function of grain size in various non-saturating magnetic fields, *Geophys. J. Int.*, *133*, 541–552.

Dekkers, M. J. (1988), Magnetic properties of natural pyrrhotite. part I. Behaviour of initial susceptibility and saturation-magnetization related rock-magnetic parameters in a grain-size dependent framework, *Phys. Earth Planet. Inter.*, *52*, 376–393.

Dekkers, M. J. (1989), Magnetic properties of natural goethite-I. Grain-size dependence of some low- and high-field related rockmagnetic parameters measured at room temperature, *Geophys. J.*, *97*, 323–340.

Dekkers, M. J., and J. H. Linssen (1989), Rockmagnetic properties of fine-grained natural low-temperature hematite with reference to remanence acquisition mechanisms in red beds, *Geophys. J. Int.*, *99*, 1–18.

Dekkers, M. J., and M. A. A. Schoonen (1996), Magnetic properties of hydrothermally synthesised greigite (Fe_3S_4)—I. Rock magnetic parameters at room temperature, *Geophys. J. Int.*, *126*, 360–368.

Dekkers, M. J., H. F. Passier, and M. A. A. Schoonen (2000), Magnetic properties of hydrothermally synthesised greigite (Fe_3S_4)—II. High- and low-temperature characteristics, *Geophys. J. Int.*, *141*, 809–819.

Dunlop, D. J. (2002), Theory and application of the Day plot (M_{rs}/M_s versus H_{cr}/H_c): 1. Theoretical curves and tests using titanomagnetite data, *J. Geophys. Res.*, *107*(B3), 2056, doi:10.1029/2001JB000486.

Dunlop, D. J., M. F. Westcott-Lewis, and M. E. Bailey (1990), Preisach diagrams and anhysteresis: Do they measure interactions?, *Phys. Earth Planet. Inter.*, *65*, 62–77.

Florindo, F., and L. Sagnotti (1995), Palaeomagnetism and rock magnetism at the upper Pliocene Valle Ricca (Rome, Italy) section, *Geophys. J. Int.*, *123*, 340–354.

Hoffmann, V. (1992), Greigite (Fe_3S_4): Magnetic properties and first domain observations, *Phys. Earth Planet. Inter.*, *70*, 288–301.

Hoffmann, V. (1993), Mineralogical, magnetic and Mössbauer data of smythite (Fe_9S_{11}), *Studia Geophys. Geod.*, *37*, 366–380.

Horng, C. S., and A. P. Roberts (2006), Authigenic or detrital origin of pyrrhotite in sediments?: Resolving a paleomagnetic conundrum, *Earth Planet. Sci. Lett.*, *241*, 750–762.

Horng, C. S., J. C. Chen, and T. Q. Lee (1992), Variations in magnetic minerals from two Plio-Pleistocene marine-deposited sections, southwestern Taiwan, *J. Geol. Soc. China*, *35*, 323–335.

Horng, C. S., M. Torii, K. S. Shea, and S. J. Kao (1998), Inconsistent magnetic polarities between greigite- and pyrrhotite/magnetite-bearing marine sediments from the Tsailiao-chi section, southwestern Taiwan, *Earth Planet. Sci. Lett.*, *164*, 467–481.

Jiang, W. T., C. S. Horng, A. P. Roberts, and D. R. Peacor (2001), Contradictory magnetic polarities in sediments and variable timing of neoformation of authigenic greigite, *Earth Planet. Sci. Lett.*, *193*, 1–12.

Kao, S. J., C. S. Horng, A. P. Roberts, and K. K. Liu (2004), Carbon-sulfur-iron relationships in sedimentary rocks from southwestern Taiwan: Influence of geochemical environment on greigite and pyrrhotite formation, *Chem. Geol.*, *203*, 153–168.

King, J. W., and J. E. T. Channell (1991), Sedimentary magnetism, environmental magnetism, and magnetostratigraphy, *U.S. Natl. Rep. Int. Union Geod. Geophys. 1987–1990*, *Rev. Geophys.*, *29*, 358–370.

Krs, M., M. Krsová, P. Pruner, A. Zeman, F. Novák, and J. Jansa (1990), A petromagnetic study of Miocene rocks bearing micro-organic material and the magnetic mineral greigite (Sokolov and Cheb basins, Czechoslovakia), *Phys. Earth Planet. Inter.*, *63*, 98–112.

Liu, Q. S., J. Torrent, Y. J. Yu, C. L. Deng, and S. K. Banerjee (2004), Mechanism of the parasitic remanence of aluminous goethites [α-(Fe, Al)OOH], *J. Geophys. Res.*, *109*, B12106, doi:10.1029/2004JB003352.

Liu, Q. S., Y. Yu, J. Torrent, A. P. Roberts, Y. X. Pan, and R. X. Zhu (2006), Characteristic low-temperature magnetic properties of aluminous goethite [α-(Fe, Al)OOH] explained, *J. Geophys. Res.*, *111*, B12S34, doi:10.1029/2006JB004560.

Mathé, P. E., P. Rochette, and D. Vandamme (1999), Néel temperature of synthetic substituted goethites and their rapid determination using low-field susceptibility curves, *Geophys. Res. Lett.*, *26*, 2125–2128.

Muxworthy, A. R., and D. J. Dunlop (2002), First-order reversal curve (FORC) diagrams for pseudo-single-domain magnetites at high temperature, *Earth Planet. Sci. Lett.*, *203*, 369–382.

Muxworthy, A. R., and A. P. Roberts (2006), First-order reversal curve (FORC) diagrams, in *Encyclopedia of Geomagnetism and Paleomagnetism*, edited by D. Gubbins and E. Herrero-Bervera, Springer, New York, in press.

Muxworthy, A. R., D. Heslop, and W. Williams (2004), Influence of magnetostatic interactions on first-order-reversal-curve (FORC) diagrams: A micromagnetic approach, *Geophys. J. Int.*, *158*, 888–897.

Muxworthy, A. R., J. G. King, and D. Heslop (2005), Assessing the ability of first-order reversal curve (FORC) diagrams to unravel complex magnetic signals, *J. Geophys. Res.*, *110*, B01105, doi:10.1029/2004JB003195.

Néel, L. (1954), Remarques sur la théorie des propriétés magnétiques des substances dures, *Appl. Sci. Res., Sect. B*, *4*, 13–24.

Newell, A. J. (2005), A high-precision model of first-order reversal curve (FORC) functions for single-domain ferromagnets with uniaxial anisotropy, *Geochem. Geophys. Geosyst.*, *6*, Q05010, doi:10.1029/2004GC000877.

Peck, J. A., R. R. Green, T. Shanahan, J. W. King, J. T. Overpeck, and C. A. Scholz (2004), A magnetic mineral record of Late Quaternary tropical climate variability from Lake Bosumtwi, Ghana, *Palaeogeogr. Palaeoclimatol. Palaeoecol.*, *215*, 37–57.

Pike, C. R. (2003), First-order reversal-curve diagrams and reversible magnetization, *Phys. Rev. B*, 104424.

Pike, C. R., A. P. Roberts, and K. L. Verosub (1999), Characterizing interactions in fine magnetic particle systems using first order reversal curves, *J. Appl. Phys.*, *85*, 6660–6667.

Pike, C. R., A. P. Roberts, M. J. Dekkers, and K. L. Verosub (2001a), An investigation of multi-domain hysteresis mechanisms using FORC diagrams, *Phys. Earth Planet. Inter.*, *126*, 11–25.

Pike, C. R., A. P. Roberts, and K. L. Verosub (2001b), FORC diagrams and thermal relaxation effects in magnetic particles, *Geophys. J. Int.*, *145*, 721–730.

Preisach, F. (1935), Über die magnetische Nachwirkung, *Z. Phys.*, *94*, 277–302.

Roberts, A. P. (1995), Magnetic characteristics of sedimentary greigite (Fe_3S_4), *Earth Planet. Sci. Lett.*, *134*, 227–236.

Roberts, A. P., and R. Weaver (2005), Multiple mechanisms of remagnetization involving sedimentary greigite (Fe_3S_4), *Earth Planet. Sci. Lett.*, *231*, 263–277.

Roberts, A. P., Y. L. Cui, and K. L. Verosub (1995), Wasp-waisted hysteresis loops: Mineral magnetic characteristics and discrimination of components in mixed magnetic systems, *J. Geophys. Res.*, *100*, 17,909–17,924.

Roberts, A. P., C. R. Pike, and K. L. Verosub (2000), FORC diagrams: A new tool for characterizing the magnetic properties of natural samples, *J. Geophys. Res.*, *105*, 28,461–28,475.

Rochette, P., P. E. Mathé, L. Esteban, H. Rakoto, J. L. Bouchez, Q. S. Liu, and J. Torrent (2005), Non-saturation of the defect moment of goethite and fine-grained hematite up to 57 teslas, *Geophys. Res. Lett.*, *32*, L22309, doi:10.1029/2005GL024196.

Rowan, C. J., and A. P. Roberts (2006), Magnetite dissolution, diachronous greigite formation, and secondary magnetizations from pyrite oxidation: Unravelling complex magnetizations in Neogene marine sediments from New Zealand, *Earth Planet. Sci. Lett.*, *241*, 119–137.

Sagnotti, L., A. P. Roberts, R. Weaver, K. L. Verosub, F. Florindo, C. R. Pike, T. Clayton, and G. S. Wilson (2005), Apparent magnetic polarity reversals due to remagnetization resulting from late diagenetic growth of greigite from siderite, *Geophys. J. Int.*, *160*, 89–100.

Schulze, D. G., and U. Schwertmann (1984), The influence of aluminum on iron oxides: X. Properties of Al-substituted goethites, *Clay Mineral.*, *19*, 521–539.

Schulze, D. G., and U. Schwertmann (1987), The influence of aluminum on iron oxides: XII. Properties of goethites synthesised in 0.3 M KOH at 25°C, *Clay Mineral.*, *22*, 83–92.

Soffel, H. C. (1981), Domain structure of natural fine-grained pyrrhotite in a rock matrix (diabase), *Phys. Earth Planet. Inter.*, *26*, 98–106.

Tarduno, J. A., R. D. Cottrell, and A. V. Smirnov (2006), The paleomagnetism of single silicate crystals: Recording geomagnetic field strength during mixed polarity intervals, superchrons, and inner core growth, *Rev. Geophys.*, *44*, RG1002, doi:10.1029/2005RG000189.

Thompson, R., and F. Oldfield (1986), *Environmental Magnetism*, 229 pp., Allen and Unwin, London.

Torrent, J., U. Schwertmann, and D. G. Schulze (1980), Iron oxide mineralogy of some soils of two river terrace sequences in Spain, *Geoderma*, *25*, 191–208.

Torrent, J., U. Schwertmann, and V. Barrón (1987), The reductive dissolution of synthetic goethite and hematite in dithionite, *Clay Mineral.*, *22*, 329–337.

van Oorschot, I. H. M., M. J. Dekkers, and P. Havlicek (2002), Selective dissolution of magnetic iron oxides with the acid-ammonium-oxalate/ferrous-iron extraction technique - II. Natural loess and palaeosol samples, *Geophys. J. Int.*, *149*, 106–117.

Weaver, R., A. P. Roberts, and A. J. Barker (2002), A late diagenetic (syn-folding) magnetization carried by pyrrhotite: Implications for paleomagnetic studies from magnetic iron sulphide-bearing sediments, *Earth Planet. Sci. Lett.*, *200*, 371–386.

Wehland, F., A. Stancu, P. Rochette, M. J. Dekkers, and E. Appel (2005), Experimental evaluation of magnetic interaction in pyrrhotite bearing samples, *Phys. Earth Planet. Inter.*, *153*, 181–190.

Wells, M. A., R. W. Fitzpatrick, R. J. Gilkes, and J. Dobson (1999), Magnetic properties of metal-substituted haematite, *Geophys. J. Int.*, *138*, 571–580.

Winklhofer, M., and G. T. Zimanyi (2006), Extracting the intrinsic switching field distribution in perpendicular media: A comparative analysis, *J. Appl. Phys.*, *99*, 08E710, doi:10.1063/1.2176598.

C. Carvallo, Institut de Minéralogie et de Physique de la Matière Condensée, Université Pierre et Marie Curie, Campus Boucicaut, 140 rue de Lourmel, F-75015 Paris, France.

L. Chang, Q. Liu, A. P. Roberts, and C. J. Rowan, National Oceanography Centre, University of Southampton, European Way, Southampton SO14 3ZH, UK. (arob@noc.soton.ac.uk)

C.-S. Horng, Institute of Earth Sciences, Academia Sinica, P.O. Box 1-55, Nankang, Taipei, Taiwan.

J. Torrent, Departamento de Ciencias y Recursos Agrícolas y Forestales, Universidad de Córdoba, Edificio C4, Campus de Rabanales, E-14071 Córdoba, Spain.